Photophysical Properties of Ruthenium(II) Tris(2,2′-Bipyridine) and Europium(III) Hexahydrate Salts Assembled into Sol−Gel Materials

Wilhelm R. Glomm,*,† Sondre Volden,† Johan Sjöblom,† and Mikael Lindgren‡

Ugelstad Laboratory, Department of Chemical Engineering, and Department of Physics, Norwegian University of Science and Technology (NTNU), N-7491 Trondheim, Norway

Received April 19, 2005. Revised Manuscript Received August 18, 2005

A series of luminescent sol−gel-encapsulated $Ru(bpy)_3Cl_2 \cdot 6H_2O$ and $EuCl_3 \cdot 6H_2O$ mixtures with $Zn(NO_3)_2 \cdot 6H_2O$ were assembled and characterized in terms of their steady-state and time-dependent photophysical properties. UV−vis absorption, steady-state emission, and FT-IR spectra were measured for the materials both in rigid and fluid media. Time-resolved luminescence measurements were also performed in order to determine radiative decay times. The samples described in this study were prepared without the addition of excess water. This was achieved by allowing the hydrolysis and condensation reactions to only consume hydration water, thus utilizing the metal salts as reactants rather than passive dopants in the system. By using this approach, the amount of hydroxyl quenchers is minimized, which can be expected to yield luminescent materials with higher luminescence quantum yields than a conventional sol−gel entrapment procedure. The emission bands of both chromophores studied here, $Ru(bpy)_3^{2+}$ and Eu^{3+}, were found to exhibit higher emission intensities, hypsochromic shifts in the emission bands, and increased decay times upon sol-to-gel conversion, which can be attributed to rigidochromism. In the case of sol−gel-encapsulated $Ru(bpy)_3^{2+}$, the complexes are thought to be surrounded by solvent molecules that interact with the silanol groups of the gel network. Thus, the Franck−Condon excited state of the complex is relaxed to a lesser extent, giving rise to the observed hypsochromic shift of the luminescence associated with the materials upon sol-to-gel conversion. A similar mechanism is proposed to be in effect for the Eu^{3+}-functionalized materials.

1. Introduction

The exceptional properties of organosilicon compounds to form siloxane polymers remain the basis for the sol−gel technique.[1] Hydrolysis and condensation of monomeric silicon alkoxide precursors upon addition of water can be described by the following three equations.

Hydrolysis:

$$\equiv Si-OR + H_2O \rightleftarrows \equiv Si-OH + ROH \quad (1)$$

Water condensation:

$$\equiv Si-OH + \equiv Si-OH \rightleftarrows \equiv Si-O-Si\equiv + H_2O \quad (2)$$

Alcohol condensation:

$$\equiv Si-OR + \equiv Si-OH \rightleftarrows \equiv Si-O-Si\equiv + ROH \quad (3)$$

where R is an alkyl group C_xH_{2x+1}.

The pH of the reaction environment highly affects the outcome. Low pH values yield fast hydrolysis and slow condensation, resulting in a three-dimensional gel. High pH yields slow hydrolysis rates and rapid condensation, resulting in a suspension of particles, in most cases with a monodisperse particle size distribution.

In 1992, Sjöblom[2] et al. showed that hydrolysis and condensation of monomeric silicon alkoxide precursors into three-dimensional gels can occur with water replaced by hydrated metal salts—in this case copper nitrate was used. A subsequent study by the same group[3] determined the hydrolysis and condensation rates of tetramethyl orthosilicate (TMOS) in alcohol solutions of $Ca(NO_3)_2 \cdot 4H_2O$ and $Ni(NO_3)_2 \cdot 6H_2O$. Here, the reactions were monitored as a function of time using FT-IR spectroscopy, and multiple linear regression was used to calculate the rate constants from the time evolution of spectra. The authors concluded that both the hydrolysis and condensation rate constants were proportional to the amount of hydration water and that the identity of the metal in the salts had a pronounced effect on the overall reaction rate. This latter observation was attributed to differences in the dissociation states in the two metal complexes studied here.

Selected rare earth and transition metal ions have luminescence properties that make them useful as optical probes of the sol−gel process, structure and properties of dendritic encapsulation and energy transfer,[4,5] as well as for luminescence and lasing applications.[6,7] Ruthenium polypyridyl complexes, and particularly Ru(II) tris(2,2′-bipyridine)

* Corresponding author. Fax: +47 73 59 40 80. E-mail: wilhelm.robert.glomm@chemeng.ntnu.no.
† Department of Chemical Engineering.
‡ Department of Physics.

(1) Brinker, C. J.; Scherer, G. W. *Sol−Gel Science*; Academic Press: San Diego, CA, 1990.
(2) Sjoblom, J.; Skodvin, T.; Selle, M. H.; Saeten, J. O.; Friberg, S. E. *J. Phys. Chem.* **1992**, *96*, 8578.
(3) Oye, G.; Libnau, F. O.; Sjoblom, J.; Friberg, S. E. *Colloids Surf., A* **1997**, *123*, 329.
(4) Pitois, C.; Hult, A.; Lindgren, M. *J. Lumin.* **2005**, *111*, 265.
(5) Kawa, M.; Frechet, J. M. J. *Chem. Mater.* **1998**, *10*, 286.
(6) Weber, M. J. *J. Non-Cryst. Solids* **1990**, *123*, 208.

10.1021/cm050825d CCC: $30.25 © 2005 American Chemical Society
Published on Web 09/29/2005

($Ru(bpy)_3^{2+}$), are among the most widely studied organometallic molecules in recent years due to their variety of attractive properties, such as strong luminescence, long excited-state lifetime, relatively high thermal and chemical stability, and appreciable reactivity of the excited state in electron and energy transfer reactions.[8,9] The luminescent excited state of $Ru(bpy)_3^{2+}$ is assigned to the metal-to-ligand charge transfer (MLCT) state, whose properties are very sensitive to the polarity and viscosity of the environment due to the MLCT character. These unique features make ruthenium polypyridyl complexes attractive for a number of applications, including optical sensors,[10−17] photosensitizers in solar energy conversion schemes,[18,19] and as probe molecules for surface quantification on metallic nanoparticles.[20,21]

Among the trivalent lanthanide ions, Eu(III) is especially useful as an optical probe of ligand or crystal field perturbations on 4f electron energy levels and radiative transition properties due to its informative luminescence spectrum.[22,23] Both the ground-state multiplet ($^7F_0$) and the principal emitting state (primarily $^5D_0$) of this ion are nondegenerate. Thus, the initial states in the $^7F_0 \rightarrow {}^5D_J$ absorption spectra and $^7F_J \leftarrow {}^5D_0$ emission spectra of Eu(III) systems remain uncomplicated even in the presence of low-symmetry ligand environments. Moreover, in emission each of the $^7F_J \leftarrow {}^5D_0$ transitions originates from separately observable spectral regions. In absorption, however, the $^7F_0 \rightarrow {}^5D_{J>2}$ transitions are sometimes obscured by intense, low-lying ligand-to-metal charge transfer (LMCT) transitions. The relative intensities of the $^7F_J \leftarrow {}^5D_0$ transitions in Eu(III) systems are of particular interest for characterizing the mechanisms responsible for 4f → 4f radiative transition probabilities. The set of $^7F_J \leftarrow {}^5D_0$ transitions have been classified according to theoretical considerations and experimental observations from a wide variety of Eu(III) systems as follows (see, e.g., Kirby et al.[23] and references therein): The $^7F_1 \leftarrow {}^5D_0$ emission is relatively strong, largely independent of the ligand environment, and primarily magnetic dipole in character. $^7F_{0,2,4} \leftarrow {}^5D_0$ emissions are essentially purely electric dipole in character, and their intensities are very sensitive to ligand structure and ligand field symmetry, with the characteristic "europium red" luminescence $^7F_2 \leftarrow {}^5D_0$ (~610 nm) being the strongest of the $^7F_J \leftarrow {}^5D_0$ transitions.[24] The $^7F_3 \leftarrow {}^5D_0$ emission exhibits mixed electric dipole and magnetic dipole character, and the (usually weak) intensity is also modulated by the details of the ligand environment. $^7F_{5,6} \leftarrow {}^5D_0$ emissions are generally very weak and have not been characterized in the same detail as the other $^7F_J \leftarrow {}^5D_0$ transitions.

A basic requirement for practical systems is that the active molecules should be immobilized in (or on) some sort of solid matrix.[25] Immobilization provides mechanical stability, as well as enabling the introduction of subtle modifications of the dopant properties due to specific host−guest interactions. One of the most often used techniques for immobilization of active molecules into solid matrixes is sol−gel encapsulation. Numerous reports exist on encapsulation of Ru(II) polypyridyl complexes in SiO_2 gels and glasses,[10,11,25−34] thin films,[8,12,13,15,25,35−38] and mixed Si−Ti oxides.[39] Also for Eu(III), there are a multitude of reports on sol−gel encapsulation in SiO_2 materials, both on systems where Eu(III) is the sole dopant[24,40,41] and on systems where a codopant, such as aluminum, is introduced.[7,42−44] The prevalent conclusion from these studies is that the excited-state properties of Ru(II) polypyridyl complexes and Eu(III) are dramatically altered by the gel matrix. Specifically, sol−gel encapsulation

(7) Costa, V. C.; Lochhead, M. J.; Bray, K. L. *Chem. Mater.* **1996**, *8*, 783.
(8) Innocenzi, P.; Kozuka, H.; Yoko, T. *J. Phys. Chem. B* **1997**, *101*, 2285.
(9) Adelt, M.; Devenney, M.; Meyer, T. J.; Thompson, D. W.; Treadway, J. A. *Inorg. Chem.* **1998**, *37*, 2616.
(10) Maruszewski, K.; Andrzejewski, D.; Strek, W. *J. Lumin.* **1997**, *72−4*, 226.
(11) Murtagh, M. T.; Kwon, H. C.; Shahriari, M. R.; Krihak, M.; Ackley, D. E. *J. Mater. Res.* **1998**, *13*, 3326.
(12) Zhang, P.; Guo, J. H.; Wang, Y.; Pang, W. Q. *Mater. Lett.* **2002**, *53*, 400.
(13) Watkins, A. N.; Wenner, B. R.; Jordan, J. D.; Xu, W. Y.; Demas, J. N.; Bright, F. V. *Appl. Spectrosc.* **1998**, *52*, 750.
(14) Zhu, H.; Ma, Y. G.; Fan, Y. G.; Shen, J. C. *Thin Solid Films* **2001**, *397*, 95.
(15) Tang, Y.; Tehan, E. C.; Tao, Z. Y.; Bright, F. V. *Anal. Chem.* **2003**, *75*, 2407.
(16) Brennaman, M. K.; Alstrum-Acevedo, J. H.; Fleming, C. N.; Jang, P.; Meyer, T. J.; Papanikolas, J. M. *J. Am. Chem. Soc.* **2002**, *124*, 15094.
(17) Wiederholt, K.; McLaughlin, L. W. *Nucleic Acids Res.* **1999**, *27*, 2487.
(18) Fleming, C. N.; Maxwell, K. A.; DeSimone, J. M.; Meyer, T. J.; Papanikolas, J. M. *J. Am. Chem. Soc.* **2001**, *123*, 10336.
(19) Fleming, C. N.; Dupray, L. M.; Papanikolas, J. M.; Meyer, T. J. *J. Phys. Chem. A* **2002**, *106*, 2328.
(20) Glomm, W. R.; Moses, S. J.; Brennaman, M. K.; Papanikolas, J. M.; Franzen, S. *J. Phys. Chem. B* **2005**, *109*, 804.
(21) Xie, H.; Tkachenko, A. G.; Glomm, W. R.; Ryan, J. A.; Brennaman, M. K.; Papanikolas, J. M.; Franzen, S.; Feldheim, D. L. *Anal. Chem.* **2003**, *75*, 5797.
(22) Kirby, A. F.; Richardson, F. S. *J. Phys. Chem.* **1983**, *87*, 2544.
(23) Kirby, A. F.; Foster, D.; Richardson, F. S. *Chem. Phys. Lett.* **1983**, *95*, 507.
(24) Matthews, L. R.; Knobbe, E. T. *Chem. Mater.* **1993**, *5*, 1697.
(25) Maruszewski, K.; Jasiorski, M.; Salamon, M.; Strek, W. *Chem. Phys. Lett.* **1999**, *314*, 83.
(26) Mongey, K. F.; Vos, J. G.; MacCraith, B. D.; McDonagh, C. M. *Coord. Chem. Rev.* **1999**, *186*, 417.
(27) Collinson, M. M.; Novak, B.; Martin, S. A.; Taussig, J. S. *Anal. Chem.* **2000**, *72*, 2914.
(28) Mongey, K.; Vos, J. G.; Maccraith, B. D.; McDonagh, C. M. *J. Sol.-Gel Sci. Technol.* **1997**, *8*, 979.
(29) Sykora, M.; Meyer, T. J. *Chem. Mater.* **1999**, *11*, 1186.
(30) Slamaschwok, A.; Avnir, D.; Ottolenghi, M. *J. Am. Chem. Soc.* **1991**, *113*, 3984.
(31) Fan, J. W.; Shi, W.; Tysoe, S.; Strekas, T. C.; Gafney, H. D. *J. Phys. Chem.* **1989**, *93*, 373.
(32) Matsui, K.; Momose, F. *Chem. Mater.* **1997**, *9*, 2588.
(33) Matsui, K.; Sasaki, K.; Takahashi, N. *Langmuir* **1991**, *7*, 2866.
(34) Castellano, F. N.; Heimer, T. A.; Tandhasetti, M. T.; Meyer, G. J. *Chem. Mater.* **1994**, *6*, 1041.
(35) Armelao, L.; Bertoncello, R.; Gross, S.; Badocco, D.; Pastore, P. *Electroanalysis* **2003**, *15*, 803.
(36) Baker, G. A.; Wenner, B. R.; Watkins, A. N.; Bright, F. V. *J. Sol.-Gel Sci. Technol.* **2000**, *17*, 71.
(37) Altamirano, M.; Senz, A.; Gsponer, H. E. *J. Colloid Interface Sci.* **2004**, *270*, 364.
(38) Murtagh, M. T.; Shahriari, M. R.; Krihak, M. *Chem. Mater.* **1998**, *10*, 3862.
(39) Momose, F.; Matsunaga, K.; Matsui, K.; Semura, S.; Kyoto, M.; Shida, A. *J. Sol.-Gel Sci. Technol.* **2002**, *23*, 79.
(40) Klonkowski, A. M.; Lis, S.; Pietraszkiewicz, M.; Hnatejko, Z.; Czarnobaj, K.; Elbanowski, M. *Chem. Mater.* **2003**, *15*, 656.
(41) Strek, W.; Sokolnicki, J.; Legendziewicz, J.; Maruszewski, K.; Reisfeld, R.; Pavich, T. *Opt. Mater.* **1999**, *13*, 41.
(42) Lochhead, M. J.; Bray, K. L. *Chem. Mater.* **1995**, *7*, 572.
(43) Hreniak, D.; Jasiorski, M.; Maruszewski, K.; Kepinski, L.; Krajczyk, L.; Misiewicz, J.; Strek, W. *J. Non-Cryst. Solids* **2002**, *298*, 146.
(44) Song, C. F.; Yang, P.; Lu, M. K.; Xu, D.; Yuan, D. R.; Liu, Z. Q. *J. Phys. Chem. Solids* **2003**, *64*, 491.

causes hypsochromic (blue) shifts of the absorption and emission bands, as well as longer radiative lifetimes and increased quantum yield upon sol-to-gel conversion. This effect can be attributed to what was originally termed rigidochromism.[45] Detailed studies since have shown this to be a general phenomenon caused by decreased rotational freedom of the entrapped molecules interacting with the silanol groups of the network and by dipole reorientation time scales.[46] The latter can be described as follows: Dipoles in the vicinity of a chromophore must reorientate in response to the immediate change in electronic structure induced by light excitation. In liquids, this reorientation is rapid, and the chromophore emits light from a relaxed excited state. In the solid state, or in viscous media, dipole reorientation times often become competitive with the excited-state decay, resulting in hypsochromic shifts in the emission spectra.

The general procedure for sol−gel encapsulation of an active species can be summarized as follows:[26] To a mixture of water (adjusted to the appropriate pH using concentrated HCl) and ethanol (containing the desired dopant complex), tetraethyl orthosilicate (TEOS) is added dropwise until the desired water/TEOS ratio is reached. Following 1 h of stirring, the solution is covered and allowed to gel and age at constant temperature for a period of up to 3 weeks, before the sample containers are opened to allow for evaporation of excess solvent. Another common monomeric silicon alkoxide precursor used in sol−gel encapsulation is tetramethyl ortosilicate (TMOS).

Here, we report the synthesis and characterization of sol−gel SiO_2 encapsulation of the systems $Zn(NO_3)_2^{2+}$ + $Ru(bpy)_3^{2+}$ and $Zn(NO_3)_2^{2+}$ + Eu(III) by direct hydrolysis and condensation of TMOS with the hydrate water of the metal salts, thus forming photonic active sol−gel materials. By allowing the reaction to only consume the hydration water, the metal salts ($Ru(bpy)_3Cl_2 \cdot 6H_2O$, $EuCl_3 \cdot 6H_2O$, and $Zn(NO_3)_2 \cdot 6H_2O$) are reactants rather than passive dopants in the system. Moreover, by not adding water to the system and by expending significant amounts of the existing hydrate water throughout the sol-to-gel conversion, the radiative quantum yield can be expected to increase, as the concentration of hydroxyl quenchers decreases significantly. Zinc nitrate was used as a nonoptically active "filler" to enable the reaction to proceed while keeping the concentration of the active species ($Ru(bpy)_3^{2+}$ or Eu(III)) low enough so as to allow transmittance through the materials and prevent self-quenching. To optimize the conditions for isotropic distribution of the active ion, metal salts with the same number of hydrate waters were chosen, as the kinetics of the sol-to-gel conversion has been shown to be highly dependent on the water-to-Si ratio.[3] The mixed sol−gel materials were found to exhibit blue-shifted emission spectra and significantly longer radiative lifetimes as compared to those of liquid solutions of the metal salts. Radiative lifetimes were also strongly affected by the H_2O/TMOS ratio. Interestingly, in mixed solutions of zinc nitrate and either Eu(III) or $Ru(bpy)_3^{2+}$, the emission spectra were blue-shifted, and the radiative lifetimes were longer than for solutions of Eu(III) or $Ru(bpy)_3^{2+}$ only. This latter observation can probably be attributed to differences in bulk viscosity between the mixed and simple solutions, respectively. The results have implications for the development of chemically integrated photonic materials.

(45) Wrighton, M.; Morse, D. L. *J. Am. Chem. Soc.* **1974**, *96*, 998.
(46) Marcus, R. A. *J. Phys. Chem.* **1990**, *94*, 4963.

2. Experimental Section

2.A. Materials. Europium(III) chloride hexahydrate (99.9%), tris-(2,2′-bipyridine) ruthenium(II) chloride hexahydrate (98%), zinc-(II) nitrate hexahydrate (98%), and tetramethyl orthosilicate (99%) were purchased from Acros Organics. Methanol (analytical grade) was purchased from Lab-Scan Ltd. All chemicals were purchased immediately before use and were used as received.

2.B. Gel Preparations. Ru(II) tris(2,2′-bipyridine) and Eu(III)-functionalized SiO_2 gels were prepared at room temperature using a procedure adopted from Øye et al.,[3] wherein TMOS was rapidly added to a MeOH solution of the metal salts $Zn(NO_3)_2 \cdot 6H_2O$ + M, where M = $EuCl_3 \cdot 6H_2O$ or $Ru(bpy)_3Cl_2 \cdot 6H_2O$. The mixture was then placed in an ultrasonicator to achieve complete dissolution and mixture of the salts with TMOS. In a typical synthesis, $Zn(NO_3)_2 \cdot 6H_2O$ (∼40 wt % of total solution) and the optically active metal salt M (M = $EuCl_3 \cdot 6H_2O$ (∼1 wt % of total solution) or $Ru(bpy)_3Cl_2 \cdot 6H_2O$ (∼0.1 wt % of total solution)) were dissolved in MeOH. TMOS was then added so as to yield the desired H_2O/TMOS ratios, varying from 2.5 to 6.5. The total mass of each sample was ∼7 g. Following thorough mixing, a fraction of each sample was transferred to a 1 cm path length polystyrene cuvette. Samples were then allowed to age for at least 1 week prior to characterization.

2.C. Spectroscopic Characterization. UV−vis spectra were collected using a Shimadzu UV-2401PC spectrophotometer. FT-IR spectra were acquired in absorbance mode using a Tensor 27 (Bruker) FT-IR spectrometer equipped with an MCT detector. The cell was a single-reflection ATR diamond crystal (MKII Golden Gate, Specac). All spectra were measured in the region of 4000−600 cm^{-1}, with an optical resolution of 1 cm^{-1}, and 32 scans were made for each measurement. Background measurements were made without sample on the ATR crystal before acquiring each spectrum. The software used was OPUS 4.2 from Bruker.

2.D. Luminescence Characterization. Time-resolved fluorescence decays were recorded using an IBH 5000 U fluorescence lifetime spectrometer system with maximum 1 nm resolved excitation and emission monochromators (5000 M). Typically, a resolution of 8−16 nm was chosen for the time-resolved measurements reported here. The system was equipped with a TBX-04 picosecond photon detection module. Luminescence emission spectra were recorded by scanning the monochromator of the detector.

The phosphorescence measurements were carried out using the IBH 5000XeF submicrosecond xenon flashlamp for Multichannel Scaling (MCS) measurements of μs−ms decay times. The shorter decay times prominent for $Ru(bpy)_3^{2+}$ were measured using time-correlated single-photon counting (TC-SPC) using an IBH Nano-LED as the excitation source with an excitation wavelength 443 nm.

The experimental data were analyzed using the IBH Data Station version 2.1 software for operation of the spectrometer and deconvolution and analysis of time decays.

3. Results

3.A. Steady-State Spectra. *3.A.1. System 1: $Ru(bpy)_3$-Functionalized SiO_2 Photonic Gels.* Steady-state emission

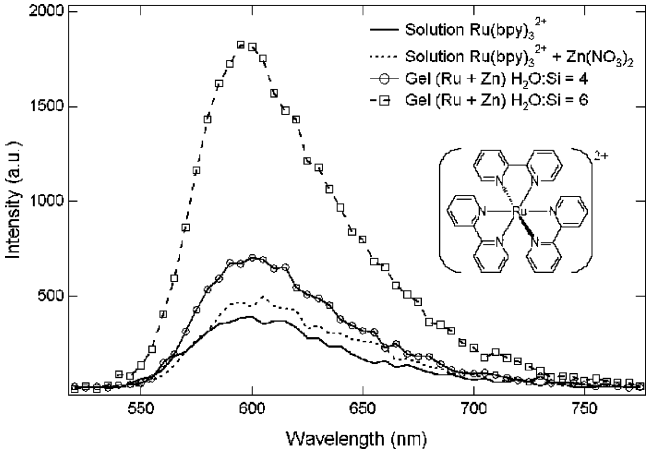

Figure 1. Phosphorescence spectra of $Ru(bpy)_3^{2+}$ under different conditions: in MeOH solution alone, with $Zn(NO_3)_2$ in MeOH solution, and in gels with varying H_2O/Si molar ratios. The concentrations of $Ru(bpy)_3^{2+}$ and $Zn(NO_3)_2$ were 0.1 and 40 wt %, respectively. The excitation wavelength was 443 nm. The molecular structure of $Ru(bpy)_3^{2+}$ is shown in the inset.

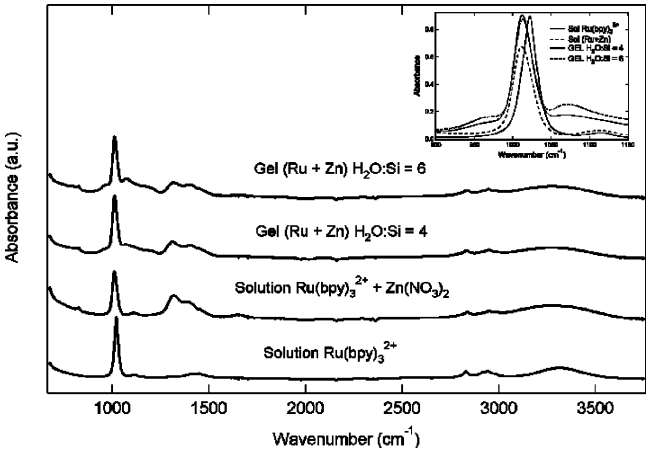

Figure 2. Infrared absorption spectra of $Ru(bpy)_3^{2+}$ under different conditions: in MeOH solution alone, with $Zn(NO_3)_2$ in MeOH solution, and in gels with varying H_2O/Si molar ratios. The concentrations of $Ru(bpy)_3^{2+}$ and $Zn(NO_3)_2$ were 0.1 and 40 wt %, respectively. An expanded view of the 1000 cm^{-1} region is shown as an inset.

spectra of $Ru(bpy)_3^{2+}$ in methanol solution (alone and in the presence of zinc nitrate) and immobilized in SiO_2 gels with zinc nitrate as a codopant are shown in Figure 1. The emission maxima centered at 595−600 nm can be attributed to phosphorescence from the triplet MLCT excited state (^{3}MLCT) to the ground state.[47] The mixed solution of $Ru(bpy)_3^{2+}$ and zinc nitrate exhibits an ∼20% increase in emission intensity as compared to that of $Ru(bpy)_3^{2+}$ only. Emission intensities of the gel samples are significantly higher than liquid-state samples and are strongly dependent on the ratio of hydrate water to Si; increasing the H_2O/Si molar ratio results in higher emission intensities. For the H_2O/Si ratios shown in Figure 1, $H_2O/Si = 4$ and $H_2O/Si = 6$, the ground state ← ^{3}MLCT intensities were found to increase by factors of ∼1.8 and 4.5, respectively, compared to that of a methanol solution of $Ru(bpy)_3^{2+}$ only. The emission maxima of the gel samples are shifted toward higher frequencies compared to that of the methanol solution of $Ru(bpy)_3^{2+}$ only, with the magnitude of the blue shift being proportional to the H_2O/Si molar ratio; a water-to-silicon molar ratio of 6 corresponds to a 5 nm shift in emission maximum, from 600 to 595 nm. Due to these systems being optimized for emission studies with respect to luminophore concentration, we were not able to collect UV−vis spectra of the ruthenium(II) tris(2,2′-bipyridine) samples. However, earlier reports[8,33] on comparable $Ru(bpy)_3^{2+}$ systems show no change in the absorption profile upon sol-to-gel conversion.

Figure 2 shows the infrared absorption spectra of $Ru(bpy)_3^{2+}$ in methanol solution (alone and in the presence of zinc nitrate) and codoped with zinc nitrate in SiO_2 gels with varying H_2O/Si molar ratios. For the methanol solutions of the hexahydrate metal salts ($Ru(bpy)_3Cl_2 \cdot 6H_2O$ and $Zn(NO_3)_2 \cdot 6H_2O$), the main observable bands are contributions from methanol and the hydrate water. From methanol, the bands can be identified (in order of ascending energy) as C−O stretch (intense peak centered at ∼1020 cm^{-1}), O−H bend (∼1440 cm^{-1}), symmetric and asymmetric C−H stretches (centered at ∼2830 and 2940 cm^{-1}, respectively), and a broad band from ∼3100 to 3500 cm^{-1} from O−H stretches.[48] The latter band also contains contributions from O−H stretches in the hydrate water (∼3000−3600 cm^{-1}). Hydrate water is also observable through the (weak) band emanating from O−H bending, centered at ∼1640 cm^{-1} (1610−1720 cm^{-1}). In the samples containing zinc nitrate, a band from O−NO_2 stretches (∼1259 to 1389 cm^{-1}) centered at ∼1317 cm^{-1} is also observable.[48] The gel samples contain several characteristics of Si−O bonds; the peak/shoulder centered at ∼940 to 950 cm^{-1} is attributed to stretching vibrations of Si−OH and Si−O^- bonds,[49] whereas the bands centered at ∼800 and ∼1070 cm^{-1} are attributed to symmetric and antisymmetric stretching vibration, respectively, of the Si−O−Si bonds.[50] In addition, O−H stretching vibrations from the silanol groups contribute to the broad band observable from ∼3000 to 3600 cm^{-1}. Differences in the H_2O/Si molar ratios as shown in Figure 2 ($H_2O/Si = 4$ and 6, respectively) can also be seen in the silanol (∼940 cm^{-1}) and siloxane (∼1070 cm^{-1}) bands; the silanol and siloxane peak intensities of the $H_2O/Si = 6$ gel sample are 49.8% and 46.3%, respectively, higher than those of the corresponding bands of the $H_2O/Si = 4$ gel sample.

3.A.2. System 2: Eu(III)-Functionalized SiO_2 Photonic Gels. Ground-state UV−vis absorption spectra of Eu^{3+} in methanol solution (alone and in the presence of zinc nitrate) and codoped with zinc nitrate in SiO_2 gels with varying H_2O/Si molar ratios are shown in Figure 3. The detected bands can, in order of descending energy, be assigned as $^7F_0 \rightarrow {}^5G_{3,4,5}$ (∼360 nm), $^7F_0 \rightarrow {}^5L_6$ (∼390 nm), $^7F_0 \rightarrow {}^5D_2$ (∼460 nm), and $^7F_{0,1} \rightarrow {}^5D_1$ (∼525−540 nm). In the gel samples, a weak band centered at ∼415 nm can also be observed, which has been assigned to the $^7F_0 \rightarrow {}^5D_3$ transition.[43] Also notable in Figure 3 is that all the spectra

(47) Durham, B.; Caspar, J. V.; Nagle, J. K.; Meyer, T. J. *J. Am. Chem. Soc.* **1982**, *104*, 4803.
(48) Silverstein, R. M.; Webster, F. X. *Spectrometric Identification of Organic Compounds*, 6th ed.; John Wiley & Sons: New York, 1998.
(49) Almeida, R. M.; Guiton, T. A.; Pantano, C. G. *J. Non-Cryst. Solids* **1990**, *121*, 193.
(50) Galeener, F. L. *Phys. Rev. B: Solid State* **1979**, *19*, 4292.

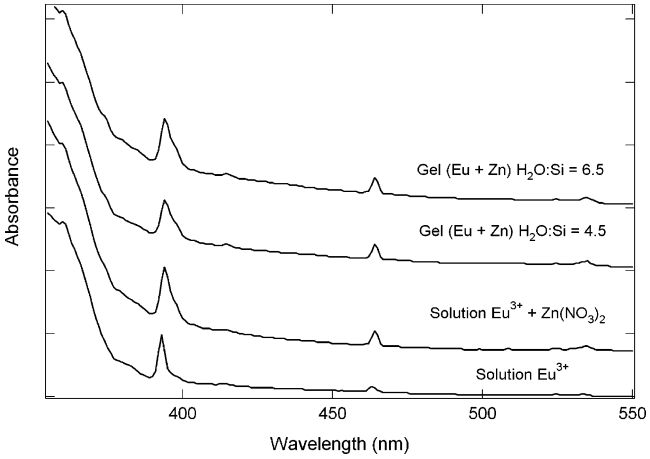

Figure 3. UV−vis absorption spectra of Eu^{3+} under different conditions: in MeOH solution alone, with $Zn(NO_3)_2$ in MeOH solution, and in gels with varying H_2O/Si molar ratios. The concentrations of Eu^{3+} and $Zn(NO_3)_2$ were 1 and 40 wt %, respectively.

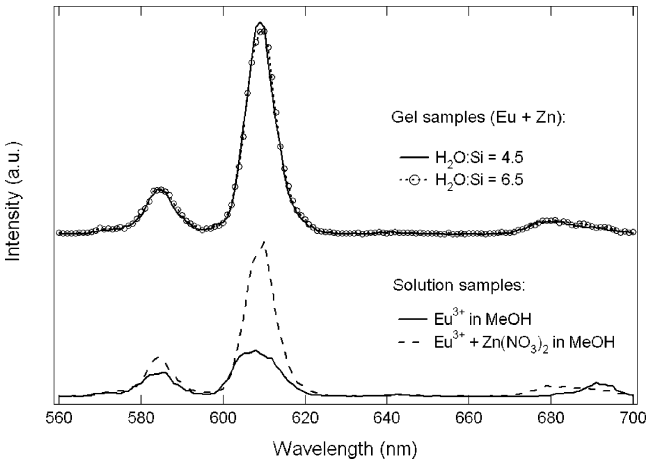

Figure 4. Steady-state emission spectra of Eu^{3+} under different conditions: in MeOH solution alone, with $Zn(NO_3)_2$ in MeOH solution, and in gels with varying H_2O/Si molar ratios. The concentrations of Eu^{3+} and $Zn(NO_3)_2$ were 1 and 40 wt %, respectively. The excitation wavelength was 390 nm.

of zinc nitrate-containing samples (both liquid-state and solid-state samples) exhibit bathochromic (red) shifts (∼3 nm) and broadening of the $^7F_0 \rightarrow {}^5L_6$ (∼390 nm) band and a slight red shift (∼2 nm) and increased intensity of the $^7F_0 \rightarrow {}^5D_2$ (∼460 nm) transition.

The corresponding steady-state emission spectra of the Eu^{3+} samples are shown in Figure 4. The excitation wavelength was 390 nm using the flash lamp and monochromator port of the spectrometer. The prominent $^7F_J \leftarrow {}^5D_0$ transitions have been assigned according to Matthews and Knobbe[24] as $^7F_0 \leftarrow {}^5D_0$ (weak band at ∼572 nm), $^7F_1 \leftarrow {}^5D_0$ (∼585 nm), the characteristic "europium red" transition $^7F_2 \leftarrow {}^5D_0$ (∼610 nm), and $^7F_4 \leftarrow {}^5D_0$ (broad band from ∼670−700 nm). In the Eu^{3+} in MeOH only sample, the weak $^7F_3 \leftarrow {}^5D_0$ (∼643 nm) transition can also be identified. The mixed solution of Eu^{3+} and zinc nitrate exhibits a 60% increase in emission intensity of the $^7F_1 \leftarrow {}^5D_0$ (∼585 nm) transition as compared to that of Eu^{3+} only, whereas maximum emission intensities of the gel samples are significantly higher than liquid-state samples, being 90% increased as compared to that of a methanol solution of Eu^{3+} only. For the "europium red" transition ($^7F_2 \leftarrow {}^5D_0$) centered

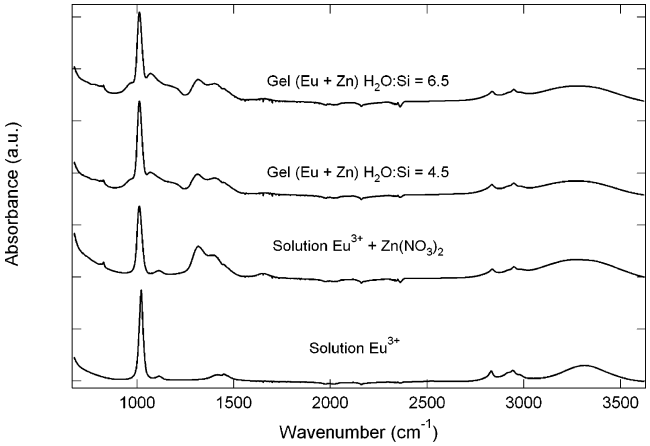

Figure 5. Infrared absorption spectra of Eu^{3+} under different conditions: in MeOH solution alone, with $Zn(NO_3)_2$ in MeOH solution, and in gels with varying H_2O/Si molar ratios. The concentrations of Eu^{3+} and $Zn(NO_3)_2$ were 1 and 40 wt %, respectively.

at 610 nm, the maximum emission intensities are even more affected by addition of zinc nitrate and by sol−gel encapsulation, with the maximum intensity being increased by factors of 3.3 and 4.5 for the mixed Eu^{3+} and zinc nitrate solution and the gel samples, respectively, as compared to a methanol solution of Eu^{3+} only. No significant effect of varying the H_2O/Si molar ratio could be observed in the steady-state emission spectra of sol−gel-encapsulated Eu^{3+}. As can be seen in Figure 4, the peak position of the $^7F_4 \leftarrow {}^5D_0$ transitions in the mixed (Eu^{3+} and zinc nitrate) solution and the gel samples exhibit hypsochromic shifts of ∼10 nm compared to that of the methanol solution of Eu^{3+} only, from ∼691 nm to ∼681 nm.

Infrared absorption spectra of Eu^{3+} in methanol solution (alone and in the presence of zinc nitrate) and codoped with zinc nitrate in SiO_2 gels with varying H_2O/Si molar ratios are shown in Figure 5. IR band assignments are the same as for the ruthenium(II) tris(2,2′-bipyridine) systems in the above section. Upon gel formation, characteristic Si−OH and Si−O−Si bands can be observed, as described above. As was determined for the $Ru(bpy)_3^{2+}$ systems, differences in the H_2O/Si molar ratios (H_2O/Si = 4.5 and 6.5, respectively) can also be seen in the silanol (∼940 cm^{-1}) and siloxane (∼1070 cm^{-1}) bands of the sol−gel-encapsulated Eu^{3+} systems. However, for the Eu^{3+} systems, the differences in band intensity do not match the corresponding bulk values as closely as was observed for the $Ru(bpy)_3^{2+}$ systems; the silanol and siloxane peak intensities of the H_2O/Si = 6.5 gel sample are 25% and 12%, respectively, higher than the corresponding bands of the H_2O/Si = 4.5 gel sample.

3.B. Time-Resolved Data. Time-resolved emission data were obtained for both the solution-state samples and the gel samples of each system. Measured lifetimes and other essential characteristics are listed in Tables 1 and 2 for the $Ru(bpy)_3^{2+}$ and Eu^{3+} systems, respectively. The values listed are derived from single-exponential decays.

3.B.1. System 1: $Ru(bpy)_3$-Functionalized SiO_2 Photonic Gels. Figure 6 shows time-resolved emission data for $Ru(bpy)_3^{2+}$ in methanol solution (alone and in the presence of zinc nitrate) and codoped with zinc nitrate in SiO_2 gels with varying H_2O/Si molar ratios. The corresponding radia-

Table 1. Emission Decay Times of $Ru(bpy)_3^{2+}$ in Methanol Solutions and in SiO_2 Gels Measured at 600 nm[a]

sample identification	H_2O/Si	decay time τ (ns)
Solution Samples		
0.1 wt % $Ru(bpy)_3^{2+}$		205.7
0.1 wt % $Ru(bpy)_3^{2+}$ + 40 wt % $Zn(NO_3)_2$		363.1
0.4 wt % $Ru(bpy)_3^{2+}$ + 28 wt % $Zn(NO_3)_2$		266.6
Gel Samples		
0.1 wt % $Ru(bpy)_3^{2+}$ + 40 wt % $Zn(NO_3)_2$	4.0	442.6
0.1 wt % $Ru(bpy)_3^{2+}$ + 40 wt % $Zn(NO_3)_2$	6.0	506.8
1.5 wt % $Ru(bpy)_3^{2+}$ + 23 wt % $Zn(NO_3)_2$	2.7	307.7
0.5 wt % $Ru(bpy)_3^{2+}$ + 36 wt % $Zn(NO_3)_2$	5.7	413.5

[a] The excitation wavelength was 443 nm.

Table 2. Emission Decay Times of Eu^{3+} in Methanol Solutions and in SiO_2 Gels Measured at 585 and 609 nm[a]

sample identification	H_2O/Si	decay time τ (μs) 585 nm	decay time τ (μs) 609 nm
Solution Samples			
1 wt % Eu^{3+}		254	262
1 wt % Eu^{3+} + 40 wt % $Zn(NO_3)_2$		272	270
Gel Samples			
1 wt % Eu^{3+} + 40 wt % $Zn(NO_3)_2$	4.5	337	379
1 wt % Eu^{3+} + 40 wt % $Zn(NO_3)_2$	6.5	339	340

[a] The excitation wavelength was 390 nm.

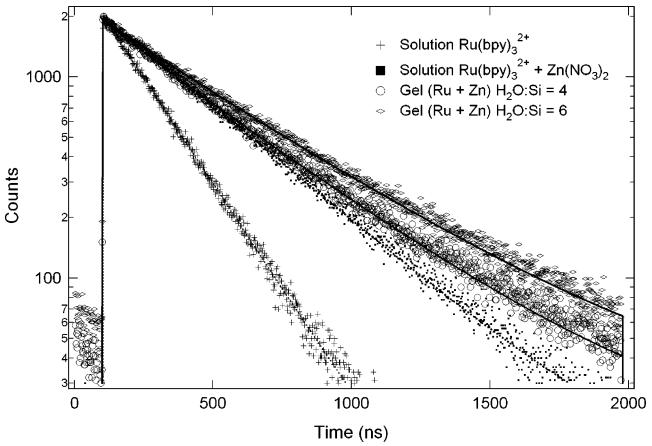

Figure 6. Time-resolved emission decay curves from $Ru(bpy)_3^{2+}$ measured at 600 nm under different conditions: in MeOH solution alone, with $Zn(NO_3)_2$ in MeOH solution, and in gels with varying H_2O/Si molar ratios. The concentrations of $Ru(bpy)_3^{2+}$ and $Zn(NO_3)_2$ were 0.1 and 40 wt %, respectively. The excitation wavelength was 443 nm. Experimental data are shown as markers, and the fits are shown as lines (solid, dashed, or dotted).

tive decay times are given in Table 1. In the systems studied here, the excited-state decay of $Ru(bpy)_3^{2+}$ is adequately modeled by single-exponential kinetics (see the fit in Figure 6). From the calculated decay times (Table 1), it can be concluded that methanol solutions of $Ru(bpy)_3^{2+}$ and zinc nitrate exhibit significantly longer decay times than a corresponding solution of $Ru(bpy)_3^{2+}$ only, with the increase in decay time being proportional to the concentration of zinc nitrate (decay time of $Ru(bpy)_3^{2+}$ only was 205.7 ns, vs 266.6 ns and 363.1 ns with 28 wt % and 40 wt % zinc nitrate, respectively). The decay time of gel-encapsulated $Ru(bpy)_3^{2+}$ is substantially longer than that of the corresponding $Ru(bpy)_3^{2+}$ + zinc nitrate solutions (see Table 1). For the gel samples in this system, the decay time is further tunable through the H_2O/Si molar ratio; an increase of the H_2O/Si ratio from 4 to 6, results in an ~15% increase of the radiative

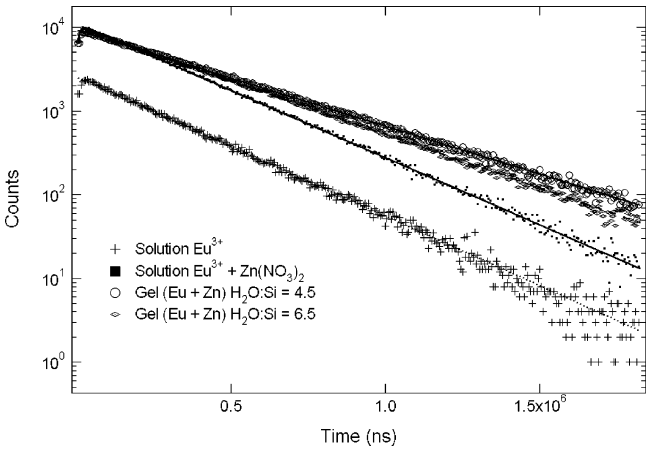

Figure 7. Time-resolved emission decay curves from Eu^{3+} measured at 585 nm under different conditions: in MeOH solution alone, with $Zn(NO_3)_2$ in MeOH solution, and in gels with varying H_2O/Si molar ratios. The concentrations of Eu^{3+} and $Zn(NO_3)_2$ were 1 and 40 wt %, respectively. The excitation wavelength was 390 nm. Experimental data are shown as markers, and the fits are shown as lines (solid, dashed, or dotted).

decay time (442.6 ns versus 506.8 ns, respectively). As can be seen from Table 1, varying the concentration of zinc nitrate in the gel samples affects the radiative decay time of $Ru(bpy)_3^{2+}$ more than tuning of the H_2O/Si molar ratio.

3.B.2. System 2: Eu(III)-Functionalized SiO_2 Photonic Gels. Time-resolved emission data for Eu^{3+} in methanol solution (alone and in the presence of zinc nitrate) and codoped with zinc nitrate in SiO_2 gels with varying H_2O/Si molar ratios are shown in Figure 7, with corresponding excited-state decay times being listed in Table 2. The excited-state decay of the Eu^{3+} systems is adequately described by single-exponential kinetics at both wavelengths where emission data was collected; 585 and 609 nm, respectively. Analogous to the $Ru(bpy)_3^{2+}$ system, mixed solutions of the luminescent metal salt (in this case Eu^{3+}) and zinc nitrate exhibit significantly longer decay times than a corresponding solution of Eu^{3+} only. Also, gel-encapsulated Eu^{3+} samples exhibit substantially longer decay times than those of the corresponding Eu^{3+} + zinc nitrate solutions (see Table 2), with the decay time being further tunable by varying the H_2O/Si molar ratio, as was the case for system 1. For the Eu^{3+} samples, both the absolute values of the radiative decay times (for all samples) and the overall trend for the H_2O/Si ratio relationship of the gel samples are dependent on what emission band was exploited (see Table 2). When monitoring the $^7F_1 \leftarrow {}^5D_0$ (~585 nm) transition, the decay time of the gel-encapsulated samples increases with increasing H_2O/Si molar ratio as for the $Ru(bpy)_3^{2+}$ system, albeit with the decay time being tunable within a much smaller range. This trend is reversed for the "europium red" transition $^7F_2 \leftarrow {}^5D_0$ (~610 nm), however; here, the excited-state decay time is reduced upon increasing the H_2O/Si molar ratio.

4. Discussion

Sol-to-gel conversion was confirmed both visually/physically and by IR spectroscopy for both the $Ru(bpy)_3^{2+}$ and the Eu^{3+}-functionalized silica gels (Figures 2 and 5, respectively). As was described in the Results, upon gel formation, several spectral characteristic of SiO_2 networks appeared

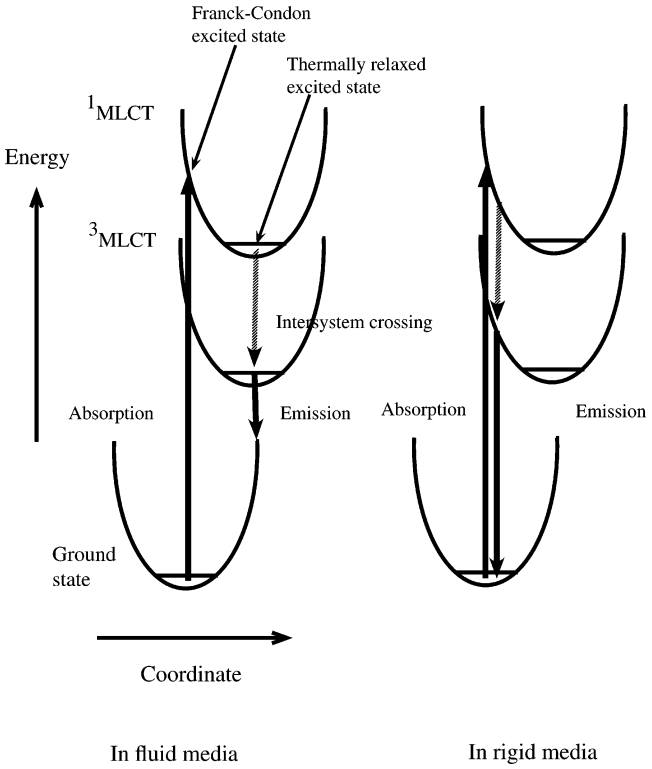

Figure 8. Schematic representation of the energy vs nuclear configuration for the electronic transitions of $Ru(bpy)_3^{2+}$ in fluid and rigid media (adapted from Innocenzi et al.[8]).

which are absent in spectra of the fluid solutions. These characteristic features include a band at ~940 to 950 cm^{-1} attributed to stretching vibrations of Si−OH and Si−O^- bonds[49] and two bands centered at ~800 and ~1070 cm^{-1}, originating from symmetric and antisymmetric stretching vibration, respectively, of the Si−O−Si bonds.[50]

Ever since Wrighton and Morse[45] reported that $Ru(bpy)_3^{2+}$ emits light at higher frequencies and exhibits longer radiative lifetimes in a rigid matrix than in fluid solution, there have been a number of reports dealing with the mechanism behind the effect originally termed "rigidochromism".[8,25,32−34] While the charge distribution of ground-state $Ru(bpy)_3^{2+}$ is symmetric, its solvated excited state has an asymmetric charge distribution due to the single-ligand localization. In a fluid solution, reorientation of solvent molecules after excitation of the complex occurs rapidly and solvate the new, highly polar MLCT excited state which is then allowed to thermally relax prior to radiative de-excitation. The thermal relaxation of the Franck−Condon (unrelaxed) excited state is schematically illustrated in Figure 8. In other words, in a fluid solution the excited state of the complex is stabilized relative to the ground state by the surrounding solvent dipoles, and the complex emits light from a relaxed excited state. On the other hand, in a rigid matrix, the solvent is not free to reorient, and thus the Franck−Condon (unrelaxed) excited state is not completely stabilized or relaxed within its lifetime. Hence, emission occurs from a higher energy level in a rigid state than in a fluid solution. This corresponds to a hypsochromic shift of the emission when the surrounding media experience sol-to-gel transition or freezing, as illustrated in Figure 8.

In the present study, phosphorescence peak shifts were detected upon sol-to-gel conversion, with the magnitude of the shift being proportional to the H_2O/Si molar ratio of the sample (Figure 1). Hypsochromic shift of the $Ru(bpy)_3^{2+}$ emission peak throughout the sol-to-gel conversion is a well-documented phenomenon in silica gels, monoliths, and thin films,[8,25,26,28,32−34,39,51] and is mainly attributed to rigidochromism. Within the concentration regime studied here, detailed UV−vis spectra could not be obtained, and thus we were unable to determine whether the sol-to-gel conversion was accompanied by shifts in the MLCT absorption band. However, in earlier studies on thin silica films[8] and sol−gel glasses[33] doped with $Ru(bpy)_3^{2+}$, the authors report that the MLCT absorption profile was unaltered as a result of sol-to-gel conversion. Assuming this holds true for the $Ru(bpy)_3^{2+}$ system studied here, this means that the change in the surrounding media only affects the relaxation of the MLCT excitation state without changing the Franck−Condon (unrelaxed) excited state.

When in a fluid solution, the $Ru(bpy)_3^{2+}$ complexes are surrounded by solvent molecules which can easily reorient when $Ru(bpy)_3^{2+}$ obtains a dipole moment upon photoexcitation. For sol−gel-encapsulated $Ru(bpy)_3^{2+}$ complexes, there are two possible states; they are either (1) still surrounded by solvent molecules, or (2) completely entrapped in the gel network, i.e., directly bonded to and fully surrounded by silanol groups. Castellano et al.[34] have reported emission anisotropy measurements on systems where $Ru(bpy)_3^{2+}$ incorporated into monolithic silica aquogels. Here, the authors concluded that the $Ru(bpy)_3^{2+}$ complexes have a residual freedom of rotational motion due to the complexes still being surrounded by solvent molecules (ethanol and water) in the silica gel. However, it should be noted that the solvent molecules surrounding the $Ru(bpy)_3^{2+}$ complex are not fully free to move or rotate due to possible interactions with the silanol groups in the surrounding network. The environment of the $Ru(bpy)_3^{2+}$ complexes can be said to experience a fluid-to-glass transition upon sol-to-gel conversion. This restriction in the freedom of movement of the solvent molecules would cause the rigidochromism and corresponding hypsochromic shift of the emission peak of the $Ru(bpy)_3^{2+}$ complex on sol-to-gel conversion. Whereas the solid (gel) state of $Ru(bpy)_3^{2+}$ complexes doped into monolithic SiO_2 aquogels can be thought of as a sol−gel entrapment where the complexes are surrounded by a "cage" of solvent molecules, the samples described in the present study are more likely to be directly bonded to and completely surrounded by silanol groups, as the hydrate water surrounding the metal salts is the only water present in the system. Thus, hydrolysis and condensation occurs solely around the hydrated metal salts, resulting in consumption of hydrate water and complete entrapment of the metal salts within the silica network. Moreover, as water is consumed from the environment surrounding the emitter, the emission quantum yield can be expected to increase, as the solvent is removed or at the very least replaced by a less polar solvent.

Unlike $Ru(bpy)_3^{2+}$, the Eu^{3+} ions do not have bulky ligands, and consequently there is no asymmetric charge distribution from single-ligand localization causing solvent reorientation from the photoexcitation-induced dipole moment. However, the basic premise of rigidochromism is still

fulfilled, as solvent dipoles in the vicinity of the chromophore, here Eu^{3+}, must reorient in response to the immediate change in electronic structure caused by light excitation. As for the $Ru(bpy)_3^{2+}$ system, sol−gel encapsulation restricts the translational and rotational freedom of the solvent molecules, thus giving rise to rigidochromism. The emission spectra of the Eu^{3+} samples (Figure 4) clearly show that the $^7F_4 \leftarrow {}^5D_0$ transition (~670 to 700 nm) is blue-shifted ~10 nm upon sol-to-gel conversion, confirming rigidochromism. Interestingly, this shift is also observed for the mixed methanol solution of Eu^{3+} and zinc nitrate (1 and 40 wt %, respectively). We believe that the shift observed for the mixed solution also can be attributed to rigidochromism, as the addition of 40 wt % zinc nitrate is going to significantly increase the solution viscosity, thus altering the time scale for solvent reorientation toward longer relaxation times, just as for the sol-to-gel conversion. A similar effect has been reported by Matsui et al.[33], where they monitored the maximum emission wavelength of sol−gel-encapsulated $Ru(bpy)_3^{2+}$ as a function of viscosity for different H_2O/Si molar ratios. Here, the authors concluded that an increase in viscosity was followed by a hypsochromic shift of the emission maximum, which confirms well with the results obtained in this study.

From Figure 4, it is evident that the emission intensities, particularly of the $^7F_1 \leftarrow {}^5D_0$ (~585 nm) and the characteristic "europium red" $^7F_2 \leftarrow {}^5D_0$ (~610 nm) transitions, increase significantly upon sol-to-gel conversion of the $EuCl_3$ containing samples. Matthews and Knobbe[24] have also studied $EuCl_3$-doped silica gels prepared via a conventional approach, wherein the lanthanide salt was added to a premade acidic solution of water, alcohol, and silicon alkoxide precursor. With the use of this approach, the $EuCl_3$-doped silica gels exhibited highly quenched luminescence, converse to what was found in the present study. This difference highlights the advantages of letting the hydrolysis and condensation reactions take place directly on the hydrate water instead of letting the reaction occur on the excess water added to the system. As discussed above, the latter, conventional approach leaves the chromophore trapped in a cage surrounded by excess water, providing efficient nonradiative deactivation of the excited state via vibronic coupling with the vibrational states of the O−H oscillators.[52−54] The luminescence properties of the chromophore are strongly dependent on the concentration of quenchers (O−H oscillators) in the proximity of the emitting species, and so by allowing the hydrolysis and condensation reactions to take place directly on the hydrate water, the local environment of the emitter is modified so as to reduce nonradiative decay mechanisms from the excited state of the chromophore.

Both the $Ru(bpy)_3^{2+}$ and the Eu^{3+} systems were found to exhibit significantly longer radiative decay times upon sol−gel encapsulation, as was expected given the vast number of preceding reports.[8−10,24−26,28,31−34,40,41,51] For the $Ru(bpy)_3^{2+}$ system, the decay time was further tunable through varying the concentration of zinc nitrate and by altering the H_2O/Si molar ratio. These findings can also be explained within the rigidochromism framework; in rigid media, the efficiency of nonradiative decay pathways is lowered compared to that in the fluid state. In the case of $Ru(bpy)_3^{2+}$, the longer decay times of samples in rigid media have been explained as follows. The excited-state properties of polypyridyl complexes of Ru(II), such as $Ru(bpy)_3^{2+}$, are often complicated by the existence of low-lying dd or ligand field states of configuration $d\pi^5 d\sigma^*$.[47,55,56] Typically, these states are formed following metal-to-ligand charge transfer (MLCT) excitation followed by a thermally activated surface crossing to the dd state. Once populated, they undergo rapid nonradiative decay or ligand loss photochemistry, which greatly limits the use of $Ru(bpy)_3^{2+}$ in molecular assemblies for energy conversion and related studies.[9] However, in rigid media, temperature-dependent decay time data have been aquired which suggest an increase in the activation barrier for the MLCT → dd surface crossing.[8−10,25] This increase of the MLCT → dd activation barrier will in turn result in longer decay times for the samples where $Ru(bpy)_3^{2+}$ resides in rigid media, namely the sol−gel-encapsulated samples and the mixed $Ru(bpy)_3^{2+}$ + zinc nitrate solutions. The latter category is included, as the presence of high concentrations of zinc nitrate results in a significant increase of viscosity as compared to that of a dilute (0.1 wt %) methanol solution of the chromophore.

5. Conclusion

A series of luminescent sol−gel-encapsulated $Ru(bpy)_3^{2+}$ + $Zn(NO_3)_2$ and Eu^{3+} + $Zn(NO_3)_2$ silica gels were assembled, and their steady-state and time-dependent optical properties were measured. The sol-to-gel conversion was confirmed both by visual inspection and by FT-IR spectroscopy. Unlike a conventional approach, wherein the chromophore is added to an acidic aqueous solution of alcohol and silicon alkoxide precursor, the samples described in this study were prepared without the addition of excess water. This was achieved by allowing the hydrolysis and condensation reactions to only consume hydration water, thus utilizing the metal salts as reactants rather than passive dopants in the system. By using this approach, the amount of hydroxyl quenchers is minimized, which can be expected to yield luminescent materials with higher quantum yields than a conventional sol−gel entrapment procedure. Zinc nitrate was used as a nonluminescent "filler" in order to boost the concentration of hydrate water in the system enough to enable the hydrolysis and condensation reactions to proceed, while keeping the concentration of chromophore low enough so as to allow transmittance through the materials and avoid self-quenching. The sol−gel materials assembled using this approach were found to exhibit higher emission intensities, hypsochromic shifts of the emission bands, and significantly longer decay times upon sol-to-gel conversion, which can be attributed to rigidochromism. Mixed methanol solutions

(51) Mongey, K. F.; Vos, J. G.; MacCraith, B. D.; McDonagh, C. M.; Coates, C.; McGarvey, J. J. *J. Mater. Chem.* **1997**, *7*, 1473.
(52) Haas, Y.; Stein, G. *J. Phys. Chem.* **1971**, *75*, 3668.
(53) Haas, Y.; Stein, G. *J. Phys. Chem.* **1971**, *75*, 3677.
(54) Haas, Y.; Stein, G. *Chem. Phys. Lett.* **1972**, *15*, 12.
(55) Hager, G. D.; Crosby, G. A. *J. Am. Chem. Soc.* **1975**, *97*, 7031.
(56) Vanhouten, J.; Watts, R. J. *J. Am. Chem. Soc.* **1976**, *98*, 4853.

of chromophore and zinc nitrate (0.1−1 and 40 wt %, respectively) also exhibited ridogochromism (longer decay times for both systems, and hypsochromic emission shifts in the case of Eu^{3+}-encapsulated sol−gel materials) due to significantly increased viscosity caused by the high concentration of zinc nitrate. However, for both systems studied, the optical properties of the materials were vastly improved upon sol-to-gel conversion. For the $Ru(bpy)_3^{2+}$-functionalized sol−gel materials, the optical properties were also determined to be tunable by altering the $Zn(NO_3)_2$/$Ru(bpy)_3^{2+}$ and H_2O/Si molar ratios.

Acknowledgment. We thank The Research Council of Norway (NFR) for financial support within the NanoMat program, Project "Dendritic Nanoporous Materials with Multifunctionality" (No. 163529/S10).

CM050825D